

GT2008-50782

A COMPARATIVE ANALYSIS OF PRESSURE SIDE EXTENSIONS FOR TIP LEAKAGE CONTROL IN AXIAL TURBINES

Akamol Shavalikul¹ & Cengiz Camci²

Turbomachinery Aero-Heat Transfer Laboratory
Department of Aerospace Engineering
The Pennsylvania State University
223 Hammond Building, University Park, PA 16802

ABSTRACT

Pressure side extensions are effective tip leakage control devices in axial flow turbines. RANS based viscous flow simulations are used to compare a number of potential aerodynamic de-sensitization devices for blade tips. The present study benefits from the past aerodynamic experiments performed in the rotating turbine rig at Penn State by Dey and Camci [14]. After a brief discussion of the computational details, a grid independency study is presented. The current study shows that a significant tip leakage mass flow rate and aerodynamic loss reduction is possible by using proper tip platform extensions located near the pressure side corner of the blade tip. A set of computations with realistic turbine rotor inlet flow conditions are performed in a linear cascade arrangement in the relative frame of reference. The boundary conditions for the computations are obtained from inlet flow measurements performed in Penn State Axial Flow Turbine Research Facility AFTRF.

INTRODUCTION

Over tip leakage flow is responsible from a significant amount of aerodynamic loss in a turbine stage. This section provides a literature review on the nature of tip leakage flow in axial flow turbines. Most shroudless turbine rotor designs require a gap between blade tips and the Casing. A comprehensive summary of the over tip leakage aerodynamics is provided by Denton [1]. The pressure difference between the pressure side and the suction sides induces the leakage flow across the tip. The over tip gap flow mixes with the main stream passage flow. The interaction of this flow results in the generation of a secondary leakage vortex near the blade suction

side corner that contains a significant loss core. Denton and Cumpsty [3] describes the effects of tip leakage flow. The leakage flow passes over the blade tip essentially without being turned. Consequently, the blade force and the work done are reduced. Tip leakage flow does not go through the usual expansion process occurring at mid-span region of the turbine passage. The leakage fluid mixing with the core flow is relatively hotter than the core fluid because of this inherent “lack of work extraction” in the tip clearance region. Bindon [2] explains how this mixing generates the aerodynamic loss. The mixing loss is typical intense within the last 40% chord length region where the fluid does not have sufficient momentum to compensate the diffusion. The flow starts to separate from the suction side corner and form a large vortical structure. The leakage flow that has a significant vortical content interacts with near casing flow, passage vortex and the blade wake flow. A tip loss model developed by Denton [1] is given in Equation 1. There are several possible means of reducing the over tip leakage flow related loss ζ , at a given relative tip clearance level t/h .

$$\zeta = \frac{2C_d}{\cos\beta_2} \left(\frac{t}{h} \right) \left(\frac{c}{s} \right) \int_0^1 \left(\frac{V_s}{V_2} \right)^3 \left(1 - \frac{V_p}{V_s} \right) \left[1 - \left(\frac{V_p}{V_s} \right) \right]^{\frac{1}{2}} \frac{dz}{c} \quad (1)$$

1. Reducing the discharge coefficient C_d
2. Modifying the rotor exit conditions
3. Changing the aerodynamic characteristics of the blade tip for raising the pressure side velocity V_p or reducing the suction side velocity V_s
4. Increasing the pitch-chord ratio s/c .

Reducing the discharge coefficient C_d : A number of studies have explored this option. Booth [4] conducted an experiment by using a water flow discharge rig to study the effects of tip geometry on the discharge coefficient C_d . According to this experiment, the knife edge geometry had the lowest C_d of 28%

1 Graduate Research Assistant
2 Prof. of Aerospace Engineering, corr. author cxc11@psu.edu

that is below the flat tip value. Bindon et al. [5] presented experimental results that were obtained in a linear cascade facility at a fixed relative gap height. When the blade tip corner radius was increased a C_d value that is 12 % higher than the blade with a plain tip was obtained. This contoured tip can reduce the flow contraction at the blade tip and the mixing loss at the suction surface. The methods, which concentrate only on reducing C_d , may not be appropriate for lower over tip leakage loss. Heyes et al. [6] studied the over tip leakage flow in two linear cascade of turbine blades. The effects of using plain tip, suction side squealer and pressure side squealer were investigated. They found that the suction side squealer gave the best reduction in C_d . The use of squealer tips for reducing tip leakage mass flow rate and loss have been reported by a number of researchers in various aspects. Camci [7] et al. showed the experimental investigation of aerodynamic characteristics of full and partial squealer rims using the Axial Flow Turbine Research Facility AFTRF at Pennsylvania State University. Various positions of a few squealer rims along the chordwise direction were investigated to reach the minimum of the aerodynamic loss. Their experimental observations from the rotating turbine rig AFTRF indicated that implementation of partial squealer rims positively affected the local aerodynamic performance by weakening the tip vortex. The term “weakening the tip vortex” was equivalent to a reduction in the momentum deficit contained in the tip vortex area. Prakash et al. [8] provided a numerical investigation of a conventional squealer tip with a straight shelf and inclined shelf near the pressure side in an effort to control the leakage flow. The computations showed that the specific shelf designs applied to the pressure side of the tip region were highly effective in weakening the tip vortex. More recent experiments performed in the rotating rig AFTRF also confirmed the beneficial influence of similar inclined shelf designs.

Modifying the rotor exit conditions: The aerodynamic characteristics of turbine blades are modified either increasing the relative exit velocity V_2 or reducing the relative angle β_2 . Yamamoto et al. [9] and Dececco et al. [10] reported that the off-loading the tip, which can change the rotor exit conditions, is able to reduce the over tip leakage flow.

Changing the aerodynamic characteristics of the blade tip for raising the pressure side velocity V_p or reducing the suction side velocity V_s : Partial shroud (winglet) geometry has the potential for increasing the pressure side velocity V_p . Patel [11] performed an experimental investigation of partial shroud tips and showed that the partial shroud tip can improve the stage efficiency by 1.2%. Booth et al. [4] studied several partial shroud geometries in a water cascade rig. The double winglet design is the most proficient design which can improve the stage efficiency by +0.6%. Yaras and Sjolander [12] investigated three different winglet geometries, pressure side winglet, suction side winglet and the double-sided winglet. The specific winglet geometries reduced the over tip leakage loss by 10%. Harvey and Ramsden [13] presented a novel design of partial shroud geometry derived from a review of past research. The winglet is predicted to significantly improve the turbine stage efficiency, by 1.2 to 1.8% at 2% relative gap height t/h . Dey and Camci [14] performed an experiment for investigating the effects of the winglet geometries upon the over tip leakage flow structure. The experimental results from the rotating rig

AFTRF showed that the pressure side extension (bump) geometry was highly effective to obtain effective over tip leakage control.

Increasing the pitch-chord ratio s/c : Denton [1] investigated the effect of changing the pitch-chord ratio, from s/c of 0.9 to 0.45, on the over tip leakage loss. For a given exit angle $\beta_2 \geq 60^\circ$ and inlet angle $\beta_1 \leq 0^\circ$, the over tip leakage decreases by 50%. Harvey and Ramsden [13] compared the over tip loss at s/c values of 1.14 and 0.57. For exit angle $\beta_2 \geq 60^\circ$ and inlet angle of 0 degree and less, the over tip leakage loss is significantly reduced by more than 44%. However, it is unacceptable to achieve lower tip leakage loss by increasing the number of rotor blades. Other sources of loss increase as well as the cost, weight and complexity of the cooling system.

The current study deals with the concept of controlling the tip leakage by using pressure side tip extension geometries. This concept was introduced by Camci et al. [7] in an experimental investigation focusing on the pressure and suction side tip platform extensions in a rotating turbine rig. It was found that properly designed pressure side extensions can reduce the over tip leakage flow mass flow rate and associated loss. Since the tested suction side tip platform extensions were not effective in reducing the tip leakage mass flow rate, the current computational effort focused on pressure side tip platform extensions. The numerical simulations of the flow for a linear cascade arrangement are performed to obtain the general characteristics of specific tip leakage flow patterns. The flow field details in the tip gap area are currently difficult to resolve by means conventional aerodynamic experimental tools. Computational simulations of tip gap flow could be beneficial in understanding leakage flow physics although the absolute accuracy of current computations may not be as good as conventional aerodynamic measurement systems. The set of computational simulations for the geometries defined in Figure 1 are as follows:

1. Baseline geometry, flat tip with out pressure side extension.
2. Bump tip, which is similar to Camci and Dey's [7] pressure side tip extension geometry.
3. Parallel pressure side extension tip; the width of the extension along the periphery is kept constant.
4. The modified-bump no.1; this geometry is obtained by shifting the tip extension of the bump tip to 50% axial chord length.
5. The modified-bump no.2; this geometry is obtained by expanding the tip extension of the bump tip from 40% to 60% axial chord length.

NUMERICAL ANALYSIS DETAILS

Governing equations : The three dimensional, steady, turbulent form of the Reynolds-averaged Navier-Stokes equations are solved by a finite volume formulation using a general purpose viscous flow solver. The rotor isothermal viscous flow calculations are performed in the relative frame of reference using measured flow conditions in the turbine rig AFTRF. The goal of the simulations is to assess the relative

total pressure change as a measure of the aerodynamic losses in the rotor. The continuity equation and momentum equations discretized are shown in Equations 2 and 3, respectively.

$$\frac{\partial U_i}{\partial x_i} = 0 \quad (2)$$

$$\rho U_j \frac{\partial U_i}{\partial x_j} = -\frac{\partial p}{\partial x_i} + \mu \frac{\partial^2 U_i}{\partial x_j \partial x_j} + \frac{\partial(-\rho \overline{u_i u_j})}{\partial x_j} \quad (3)$$

Turbulence model : From Equation 3, the Reynolds stress tensor $-\rho \overline{u_i u_j}$ components are modeled by using the Boussinesq hypothesis.

$$-\rho \overline{u_i u_j} = -\rho \frac{2}{3} k \delta_{ij} + \mu_t \left(\frac{\partial U_i}{\partial x_j} + \frac{\partial U_j}{\partial x_i} \right) \quad (4)$$

The standard k-ε model, proposed by Launder and Spalding is employed to model the turbulence. The Reynolds stress is modeled in terms of two turbulence parameters, the turbulent kinetic energy k and the turbulent energy dissipation rate ε. The turbulent kinetic energy equation is shown in Equation 5.

$$\rho U_i \frac{\partial k}{\partial x_i} = \mu_t \left(\frac{\partial U_j}{\partial x_i} + \frac{\partial U_i}{\partial x_j} \right) \frac{\partial U_j}{\partial x_i} + \frac{\partial}{\partial x_i} \left\{ \left(\mu + \frac{\mu_t}{\sigma_k} \right) \frac{\partial k}{\partial x_i} \right\} - \rho \epsilon \quad (5)$$

The standard smooth-wall functions, proposed by Launder and Spalding, are used to represent the near wall flow characteristics. The law-of-the-wall for mean velocity yields as the following equation.

$$\frac{U_p C_\mu^{1/4} k_p^{1/2}}{\tau_w / \rho} = \frac{1}{K} \ln(E y^*) \quad \text{where} \quad y^* = \frac{\rho C_\mu^{1/4} k_p^{1/2} y_p}{\mu}$$

Discretization and boundary conditions : The governing equations are solved by using a finite volume technique with a second-order upwind discretization scheme. All simulations in this study are performed by using the commercially available general purpose flow solver Fluent 6.3.

Figure 2 represents the grid system, which is equivalent to the linear cascade version of a turbine passage in AFTRF. The non-dimensional tip gap is $t/h = 2\%$ where $h = 123$ mm. Passage flow details of this cold flow turbine are presented in Lakshminarayana, Camci, Halliwell and Zaccaria [16]. These unstructured grids with grid-clustering in the near wall and tip gap region are generated by using the general purpose grid generator software Gambit. At the inlet, the velocity boundary layer profile is specified. The values of k and ε imposed at the inlet boundary are based on measured turbulence intensity and length scale from the AFTRF, [16]. The simulations performed in this study correspond to a Reynolds number of 291,000 based on axial chord length at the tip diameter and mass averaged inlet velocity. The turbine outer casing in this linear cascade computation is defined as a moving wall to simulate the blade rotation. The relative velocity of the casing is computed from the turbine rotational speed of $N=1320$ rpm with respect to the blade.

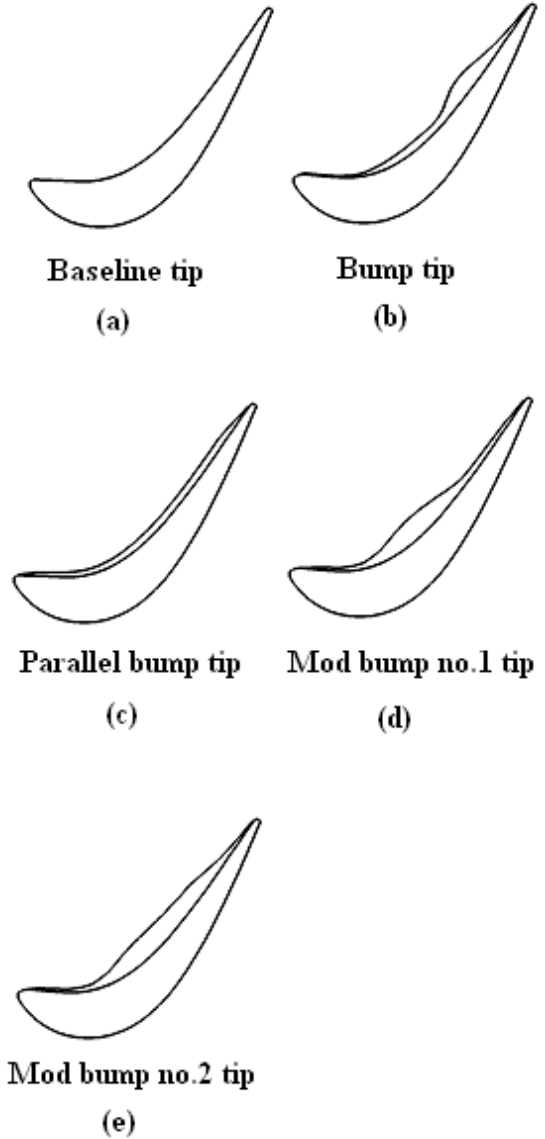


Figure 1 Schematic of the tip geometries

All other walls in this computation are set to a stationary condition. To avoid the interference of the flow structure inside the computational domain, the outlet boundary should be located at three chord lengths downstream away from the trailing edge. The flow is simulated with periodic boundary conditions imposed along the boundaries in the circumferential direction.

Convergency and grid independency : The acceptable convergence of all cases is achieved when all parameters residual levels are lower than the order of 10^{-5} . The converged simulations usually needed approximately 1,000 iterations. To find the appropriate grid density, a grid independency study is performed. The grid independency is checked by comparing all solutions of the baseline tip from 3 different grid densities which are 720,000, 1,000,000 and 1,200,000 grid nodes. The static pressure at 50% chord length of all different grid

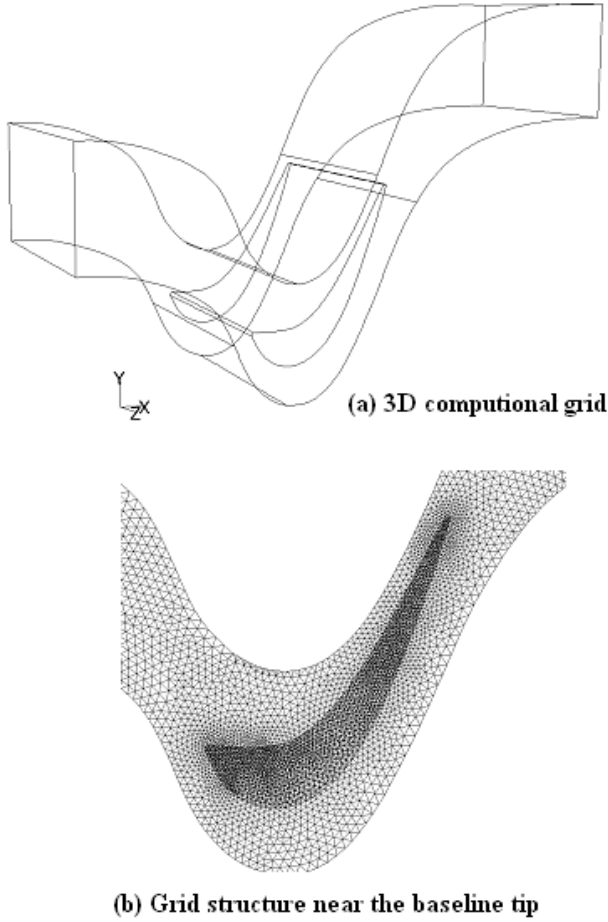


Figure 2 Schematic of the grid for the flow simulation

densities are plotted as shown in Figure 3. It can be seen that the suction side static pressure at 720,000 grid nodes case has a grid dependent solution. When the grid density is increased to 1,000,000 a significant change in the pressure distribution is observed. Once 1,000,000 grid node number is exceeded the solution becomes grid independent. To achieve a reasonable grid independency, all simulations in this study are thus undertaken by using 1,000,000 grid nodes.

RESULTS AND DISCUSSION

Static pressure distribution on the tip surface : Referring to many over tip leakage investigations, the pressure difference of the suction side and the pressure side can drive the flow through the tip gap. Thus, the static pressure distributions on the tip platform are of prime importance. In this section, the effects of the different tip geometry on the pressure distribution are examined. The pressure distribution is quantified by using the static pressure coefficient C_p , as defined in Equation 7. The C_p distributions on blade tip platform clearly show the extent of the pressure driven flow, the separation zone near the pressure side corner and trailing edge region where pressure on both pressure side and suction side are very close to each other.

$$C_p = \frac{(P - P_{inlet})}{0.5 \times \rho \times V_{inlet}^2} \quad (7)$$

A large and negative value of the pressure coefficient C_p corresponds to a low pressure difference and vice versa. Thus, the area which has the lower value of C_p would have more potential for the tip leakage drive (green and blue zones).

Figure 4 depicts the static pressure coefficient contours on the blade tip for the baseline and other “pressure side extension” tip designs. It shows that the first 20% axial chord length from the leading edge region has high C_p meaning that the amount of over tip leakage flow in this area is relatively low. The red-orange zone near the leading edge does not have strong pressure gradients to result in significant tip leakage. The high level of over tip leakage flow, which is represented in regions with blue-green color, occurs in between 20% and 70% of axial chord length region. The last 20% axial chord length region near the trailing edge experiences a relatively low tip leakage flow. The C_p distribution on the blade tip especially near the pressure side corner is modified by the pressure side extension tip designs. Dark blue zones at the leakage flow entrance areas are almost eliminated in modified bump designs shown in Figure 4 (d) and (e).

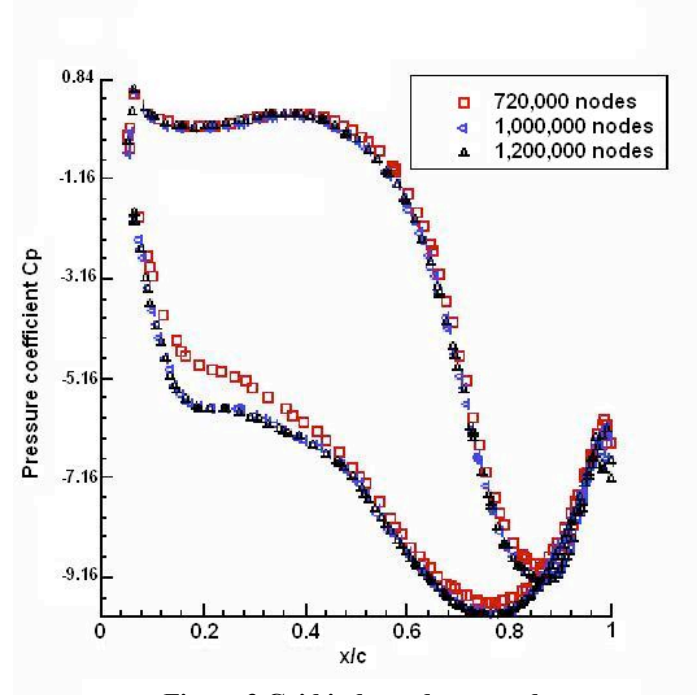


Figure 3 Grid independency study, the static pressure at 50% blade height

Clearly, the pressure side extension tips have higher C_p on the tip leakage dominant area. The dark blue color in the dominant leakage region of the baseline tip changes to the light blue color (even green) for all pressure side extension tips. With pressure side extension tips, blade tip platform static pressure field shows a weakened pressure driven flow characteristic.

Bump tip : A comparison of the baseline tip and the bump tip shown in Figure 4a and 4b indicates that the dominant tip

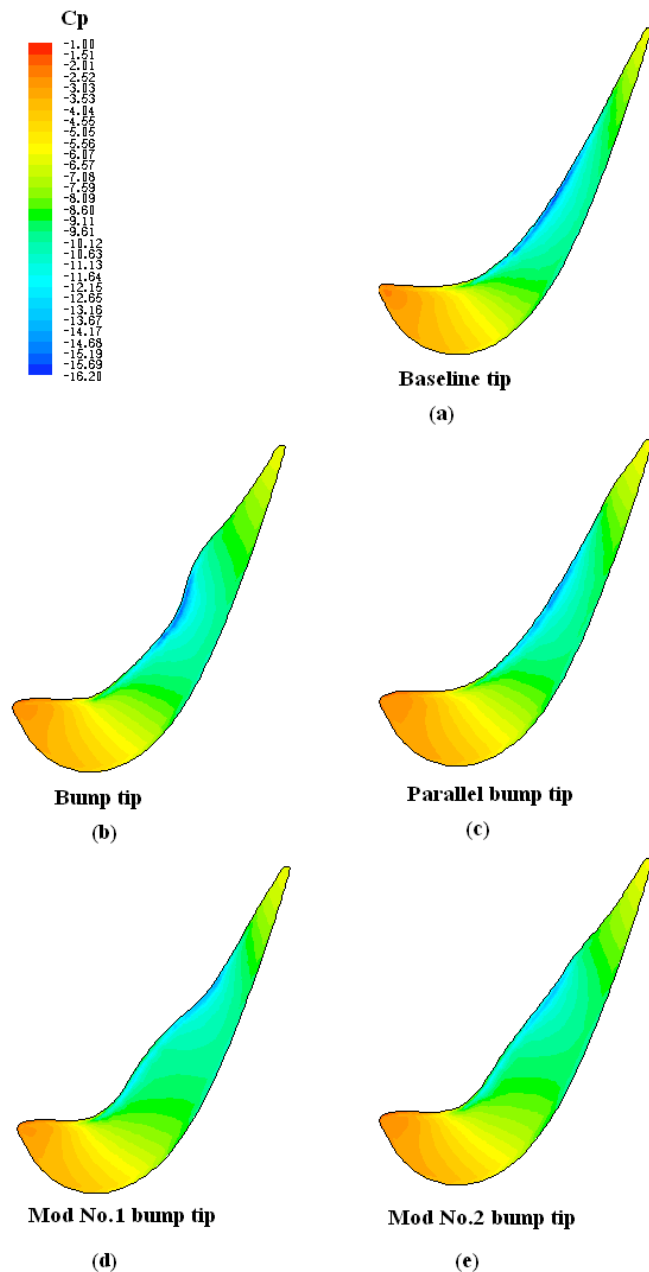


Figure 4 Contours of static pressure coefficient on the blade tip surface

leakage region (dark blue) of the bump tip is smaller than that of the baseline tip. As a result of the smaller tip leakage dominant area, the mass flow rate of over tip leakage decreases. However, the pressure distribution from the baseline tip and bump tip shown in Figure 4 suggested that further improvements to limit the leakage mass flow rate are still possible. Other pressure side extension geometries are designed to minimize the leakage mass flow rate in the tip gap area.

Parallel extension tip : Figure 1 and 4c show the parallel extension tip where the pressure side extension has almost constant width from the leading edge to trailing edge region. This design was generated with the expectation that bump tip's

leakage control features could be repeated in other chordwise positions of the tip profile. Parallel bump tip results in a visible improvement in leakage control when compared to bump tip and baseline tip.

Modified bump tip No.1 : Moving the pressure side extension of the bump tip to the lowest C_p location of the baseline tip can also be a possible option to reduce the tip leakage flow characteristic as seen in modified bump tip no. 1 as shown in Figure 4.d. According to Figure 4.c, the parallel bump tip can eliminate the narrow dark blue zone observed near the pressure side corner in Figure 4.b. The leakage region still covers a wide area. However, Figure 4.c indicates a weakened leakage flow zone in the gap area. The very low static pressure zone (dark blue) apparent near the pressure side corner in general is a measure of the mass flow rate of the leakage flow entering into the tip gap region. When the leakage flow turns around the pressure side corner, it is known that there is a narrow flow separation zone and possible attachment near the pressure side corner. Modified bump tip No.1 design effectively eliminates very low static pressures resulting from significant leakage mass flow rate.

Modified bump tip No.2 : This design idea is based on the fact that the individual leakage control features of the “bump tip” and “modified bump tip No.1” could be effectively combined into one tip extension design. A much wider tip platform extension with a wider chordwise coverage as shown in Figure 4.e is incorporated from $x/c=0.2$ to $x/c=0.8$. There is no dark blue color contained in the C_p contour map of the “modified bump tip No.2” indicating that the excessive leakage or high flow acceleration around the pressure side corner is under control. The extent of the dark blue areas near the pressure side corner is an indication of the strength of the leakage flow passing from the tip gap region.

Mass flow rate across the tip gap : As a quantitative evaluation, the local over tip leakage mass flow rate across the tip platform camberline is plotted in function of axial chord length in Figure 5. The evaluation is performed over equally formed rectangular areas aligned with the camberline of the tip profile. The computed leakage velocity vectors are integrated over individual rectangular areas to determine the local leakage mass flow rate passing from the tip gap region over the camberline. The leakage mass flow rate continually increases from the leading edge to a maximum value around $x/c=0.65$ for the baseline tip. The peak leakage location and the amount of the maximum leakage mass flow rate are different for the “bump tips” and “parallel extension tip”. The mass flow rate at the trailing edge region falls rapidly after $x/c=0.85$. The specific design of the tip platform extension does not influence the local leakage mass flow rate after $x/c=0.85$. The “bump tip” and “parallel tip” local leakage character is the same before $x/c=0.70$. Both treatments provide a considerable gain in reducing tip leakage mass flow rate. The “bump tip” alone is the most effective treatment only between $x/c=0.70$ and 0.85 .

When the location of the bump is moved towards the leading edge, the “modified bump tip No.1”, a highly effective leakage reduction is obtained for the mid chord area between $x/c=0.40$ and 0.70 . The most effective leakage reduction is obtained in a much wider area using the “bump tip” and “modified bump tip no.1”. This design is named “modified bump tip no.2” and it is

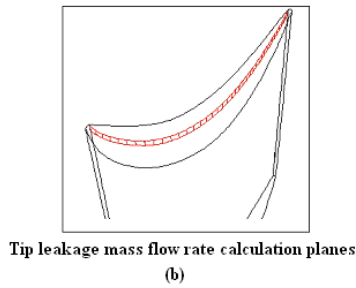
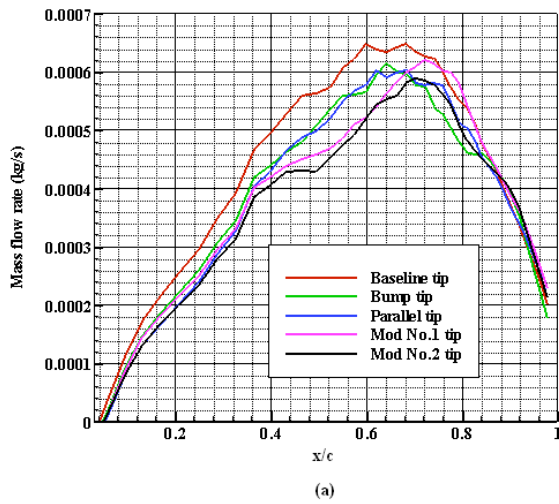


Figure 5 The mass flow rate across the tip gap

the most effective treatment providing leakage reduction between $x/c=0.35$ and 0.85 .

When the computed local mass flow rates shown in Figure 5 are integrated over the tip gap boundary defined over the blade tip camberline as shown in Table 1, the baseline tip case has the maximum leakage mass flow rate. Reduced leakage mass flow rates can be obtained from all of the pressure side extension tip geometries presented in Figure 1.

	Mass flow rate (kg/sec)
Baseline tip	0.01757
Bump tip	0.01606
Parallel bump tip	0.01613
Mod. No.1 bump tip	0.01626
Mod. No.2 bump tip	0.01552

Table 1 Mass flow rate over the blade tip camberline planes

Figure 5. shows that, the maximum tip leakage flow region of the “baseline tip”, the “bump tip” and the “parallel tip” are almost at the same location at about $x/c=0.60$. The high tip leakage region of the “modified bump tip No.1” and “modified bump tip No.2” are shifted to 70 % chord length.

Re-circulatory tip flow patterns in cross-stream planes : Figures 6, 7 and 8 depict computationally generated flow visualization patterns inside three selected planes located at $x/c=0.30$, 0.60 and 0.90 respectively. Figure 6 shows the exact

alignment of the three visualization planes. The visualization plane is defined as a plane that is approximately normal to the mean flow direction in the passage. The visualization planes are aligned such that they contain most of the tip leakage flow patterns originating from the pressure side corner. The leakage flow is from the right hand side (PS) of each figure to left hand side (SS) corner. The leakage flow entrance area near the pressure side corner of the tip and the interaction of the leakage jet emanating from the tip gap area, its interaction with the passage vortex and the casing wall are mostly contained in selected planes. The visualizations are generated by using the pathlines based on the velocity components in the visualization plane and colored by the level of total pressure coefficient C_{p0} . The numerically generated pathline based flow visualizations are conceptually equivalent to “smoke flow visualizations” obtained on extremely thin laser sheets that are normal to the blade tip platform.

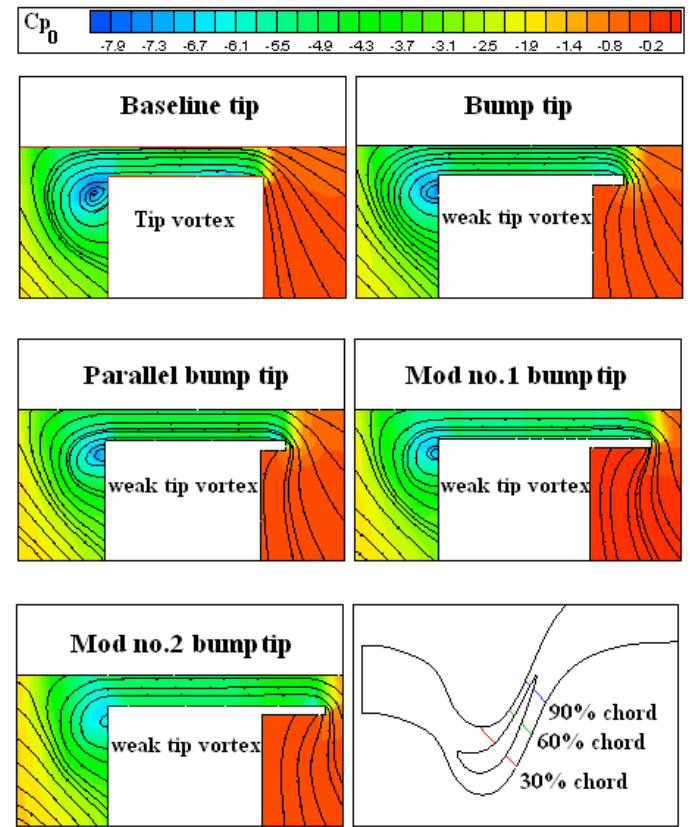


Figure 6 Leakage flow patterns in the visualization plane at $x/c=0.30$

The total pressure coefficient is described as follows:

$$C_{p0} = \frac{(P_{total} - P_{total,inlet})}{0.5 \times \rho \times V_{inlet}^2} \quad (8)$$

Modified tip vortex structure at $x/c=0.30$: The leakage flow patterns of all pressure side extension tip geometries obtained at $x/c=0.30$ are similar to the baseline tip results except the gap entrance region. The specific tip platform extension geometry near the pressure side corner determines the shape of entrance area pathlines. The tip leakage flows from the pressure side to

suction side of the blade and then mixes with the main passage flow generating tip vortex. The five specific treatments displayed in Figure 6 all show a slight reduction on the strength of the tip vortex because of the tip platform extensions. The dark blue zone in the core of the resulting tip vortex becomes a light blue region indicating that the total pressure deficit in the core of the baseline tip is slightly reduced.

Modified tip vortex structure at $x/c=0.60$: A large amount of tip leakage flow normally mixes with the main passage flow and generates a strong tip vortex for the baseline tip as shown in Figure 7. The tip vortex dominated area at $x/c=0.60$ contains higher momentum deficit and energy loss over a large area when compared to $x/c=0.30$. The bump tip geometry and the parallel bump tip geometry provide a visible reduction in the area coverage of the tip vortex in comparison the baseline

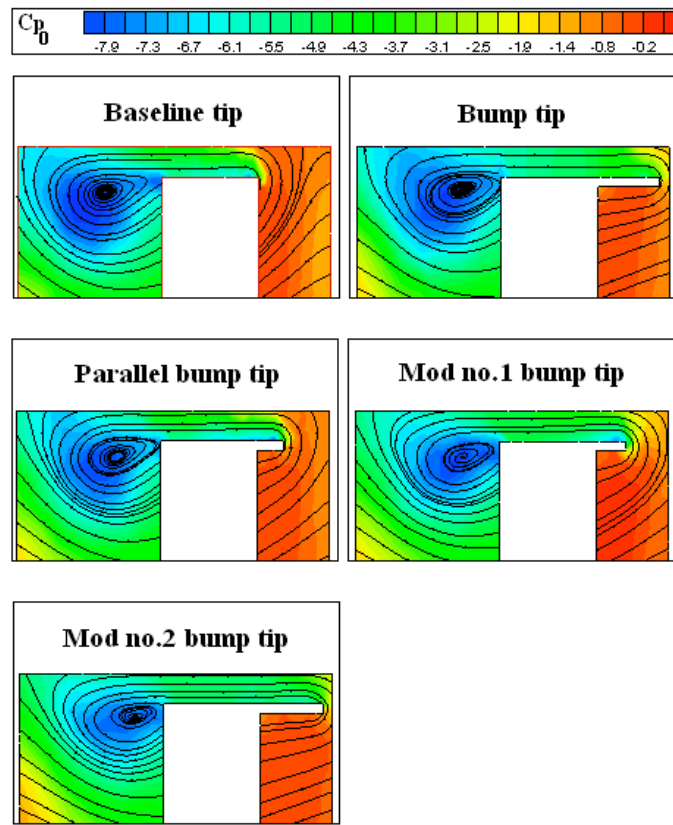


Figure 7 Leakage flow patterns in the visualization plane at $x/c=0.60$

tip. The momentum deficit (dark blue zone) in the core of the tip vortex is also visibly recovered. Thus, these suggested blade tip geometries are able to reduce the overall leakage mass flow rate and the aerodynamic losses associated with the tip vortex residing near the suction side corner of the blade. On the other hand, the modified no.1 and modified no.2 bump tips produce the smallest size of the tip vortices and their cores move closely toward the suction side surface.

Modified tip vortex structure at $x/c=0.90$: Figure 8 presents the leakage flow patterns inside the visualization plane at $x/c=0.90$. Even though the over tip leakage flow mass flow rate in the trailing edge region is relatively small, the level of loss is

extremely high. Figure 8 shows the large vortex and the high negative total pressure coefficient cover almost the whole cross section plane. The tip vortices for all geometries are now located further away from the blade tip. At $x/c=0.90$, the leakage mass flow rate from the pressure side to suction side corner is much smaller compared to planes located at $x/c=0.60$ and 0.30 . The tip vortex core is large at this station mainly because of the previous leakage mass flow contributions that already formed a distinct tip vortex structure well before $x/c=0.90$ location. Comparisons of the results from the five tip platform designs indicate that the lowest level of total pressure loss occurs when modified no.2 bump tip geometry is used. The total pressure contours and the computed pathlines do not coincide at this location. Because of the significant reduction of the leakage mass flow rate in the trailing edge zone, the local

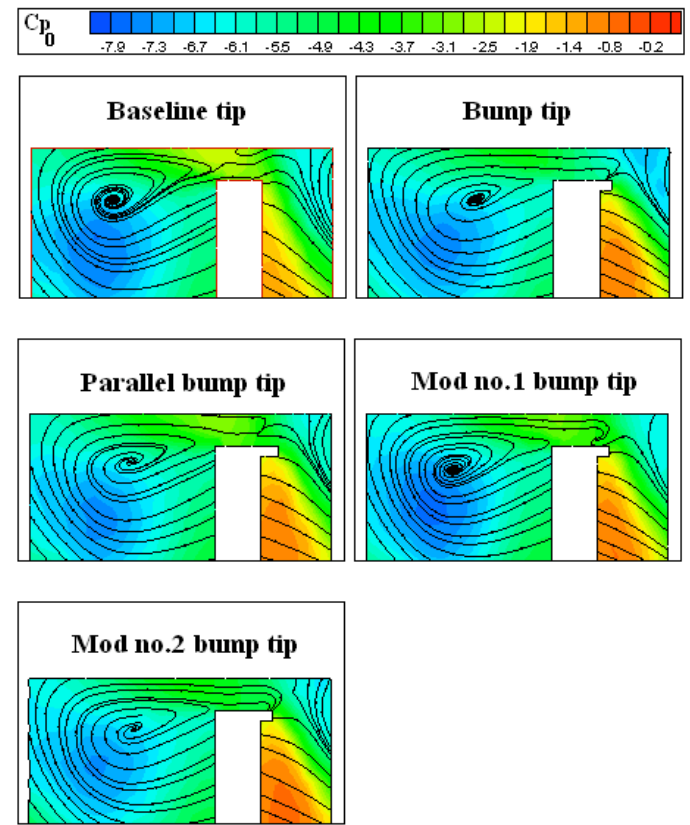


Figure 8 Leakage flow patterns in the visualization plane at $x/c=0.90$

leakage mass flow rate is not significant. The local cross stream velocities in the trailing edge area are minimal. However, the tip vortex structure already defined at earlier stations still exhibits its total pressure character as shown by the blue loss core. The tip vortex core starts diffusing at $x/c=0.90$ but it is still highly visible in the cross stream plane.

The total pressure field and losses at exit plane : Figure 9 presents the relative total pressure distribution at the exit plane behind the blade row for all pressure side extension designs. The exit plane is defined as the plane that is normal to the main flow direction at 120% chord length as shown in Figure 9. At this axial position, the tip leakage vortex, the wake and the

passage vortex fluid show strong turbulent mixing and diffusive character. The local level of the relative total pressure coefficient can be related the amount of aerodynamic losses originating from various tip treatments presented in this paper. The aerodynamic losses originating from the dissipation of the mean kinetic energy into thermal energy can be estimated by using local relative total pressure in an isothermal

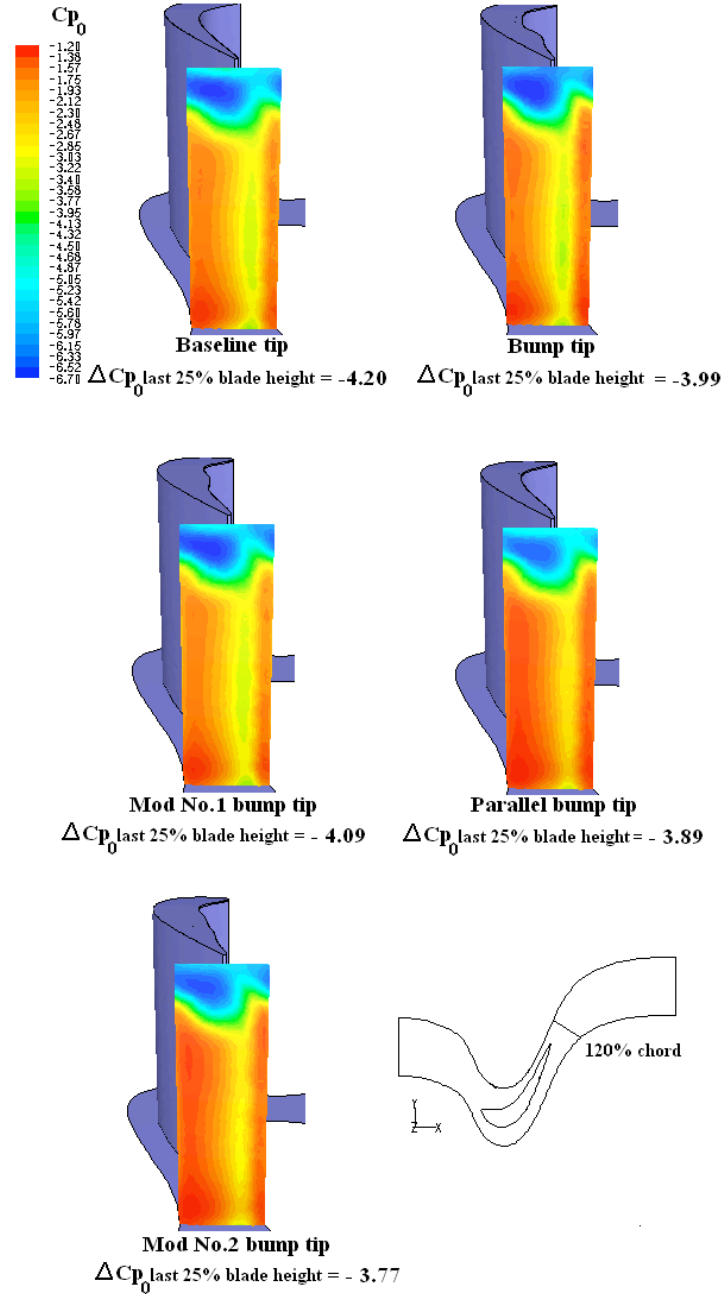


Figure 9 Total pressure coefficients at the exit plane

viscous flow simulation in the relative frame of reference. The red color shows the relative total pressure at the inlet of the rotor indicating the lowest loss level. Dark blue indicates the highest level of losses at the exit plane.

The best approach to quantify the effectiveness of a tip treatment is to calculate the mass averaged relative total pressure coefficient over the area of interest in the exit plane.

The specific area chosen for the evaluation of various tip extensions is the area in the last 25 % of the blade height.

$$\Delta C_{P0, \text{last 25\% blade height}} = \bar{C}_{P0 \text{ exit plane}} - \bar{C}_{P0 \text{ inlet}} \quad (9)$$

$$\Delta C_{P0} = \Delta C_{P0, \text{last 25\% blade height}}$$

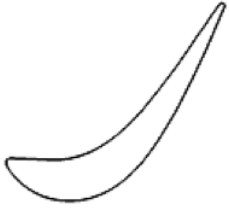




 Baseline tip $\Delta C_{P0} = -4.20$	 Bump tip $\Delta C_{P0} = -3.99$
 Parallel bump tip $\Delta C_{P0} = -4.09$	 Mod bump no.1 tip $\Delta C_{P0} = -3.89$
 Mod bump no.2 tip $\Delta C_{P0} = -3.77$	

Table 2 Comparison of aerodynamic losses
(change in non-dimensional relative stagnation pressure)

This area fully contains the leakage flow dominated zone and a significant portion of the blade wake and core fluid between the wakes. Since the leakage vortex and passage vortex has a significant interaction in the passage, the rest of the passage is affected from this interaction. Slight variations in the blade wakes is closely related to the flow structure change in the tip

leakage area. Table 2 presents the area averaged total pressure loss as the difference of total pressure loss coefficients between the exit plane and inlet plane in the relative frame of reference.

The “*bump tip*” flow modifications provide a good improvement when compared to the baseline case as shown in Figure 9 and Table 2. This computational result is consistent with experiments performed in the same turbine rig by Dey and Camci [14]. An aerodynamic loss level of $\Delta C_{p0} = -3.99$ is obtained from the bump tip. The “*baseline tip*” loss level is at $\Delta C_{p0} = -4.20$.

The “*parallel bump tip*” based on the idea that a much longer tip extension in chordwise direction may well provide more effective tip loss control. The flow computations show a slightly better loss control than the baseline case. However the parallel bump tip does not perform as well as the bump tip. [$\Delta C_{p0} = -4.09$]

The “*modified bump no.1*” tip is a design to test the location of the maximum bump location. When the maximum bump location is moved to a mid chord position, a significant loss control is achieved when compared to baseline, bump, parallel bump tip designs. [$\Delta C_{p0} = -3.89$]

The “*modified bump no.2*” tip is a design combining the benefits of the “*bump tip*” and the “*modified bump no.1 tip*” design as shown in Figure 1.e. This design provides the most significant gain in terms of controlling the tip aerodynamic losses. A ΔC_{p0} of -3.77 results in when compared to that of the baseline case $\Delta C_{p0} = -4.20$.

Conclusions

The current study presents computational viscous flow simulations of various tip platform extension designs for the control of aerodynamic losses originating from tip leakage flows in an axial flow turbine.

Carefully measured rotor inlet conditions and rotor geometry is used in the linear cascade simulations of AFTRF rotor conditions in the relative frame of reference.

The four new tip platform designs are compared to the AFTRF baseline blade tip that does not have any tip platform extensions. All four cases show measurable improvement in reducing tip leakage related losses.

The quantitative estimations of the over tip leakage flow are achieved by calculating the mass flow rate across the mean camber line region. All of the pressure side extension tips produce reduced mass flow rates across the mean camber line region. The most effective tip geometry to reduce the mass flow rate across the camber line region is the “*modified no.2 bump*” tip.

The flow leakage patterns at 3 chordwise visualization planes are presented to show that the pressure side extension tips are able to weaken the tip vortex structure.

The “*bump tip*” flow modifications provide a good level of loss reduction when compared to the baseline case. This computational result is consistent with experiments performed in the same turbine rig by Dey and Camci [14].

The “*parallel bump*” provides more effective tip loss control. The flow computations for this case show a slightly better loss control than the “*baseline case*”. However, the “*parallel bump tip*” does not perform as well as the “*bump tip*”. [$\Delta C_{p0} = -4.09$]

The “*modified bump no.1*” tip is obtained when the maximum bump location is moved to a mid chord position. A significant loss control is achieved when compared to baseline, bump and parallel bump tip designs. [$\Delta C_{p0} = -3.89$]

The “*modified bump no.2*” tip is a design combining the leakage control benefits of the “*bump tip*” and the “*modified bump no.1 tip*” design. This design provides the most significant aerodynamic loss reduction.

The prediction of the aerodynamic losses in the absolute frame of reference including all rotational flow effects and an annular geometry is currently in progress. This future viscous flow study includes a complete NGV stationary flow simulation and a blade passage computation that is connected to stationary frame through a mixing plane analysis.

Aerothermal and structural aspects of integrating tip platform extensions into hot turbine environment is a topic for future study in our laboratory. The feasibility of the current aerodynamic designs need to be demonstrated for the hot gas environment.

Nomenclature

c	=	Chord
C_d	=	Discharge coefficient, ratio of actual to ideal mass flow
C_p, C_{p0}	=	Static and total pressure coefficients
ΔC_p	=	Aerodynamic loss coefficient
C_μ	=	Constant, 0.09
E	=	Empirical constant, 9.793
t	=	Tip clearance
h	=	Rotor blade height
k	=	Turbulent kinetic energy
K	=	Von Karman constant
k_p	=	Turbulence kinetic energy at point p
N	=	Turbine rotational speed rpm
P_{total}	=	Total pressure
P	=	Static pressure
RANS	=	Reynolds averaged Navier-Stokes
s	=	Pitch
t	=	Tip clearance
u_i	=	Fluctuating velocity component
U_i	=	Mean velocity component
u_p	=	Mean velocity of the fluid at point p
V_2	=	Relative exit velocity
V_p	=	Pressure side velocity
V_s	=	Suction side velocity
y_p	=	Distance from point p to the wall
x, y, z	=	Cartesian coordinate system

β	=	Relative angle
ε	=	Turbulent dissipation rate
ρ	=	Density
μ	=	Viscosity
μ_t	=	Turbulent (or eddy) viscosity
ξ	=	Kinetic energy loss coefficient
σ_k	=	Constant, 1

Turbine Cascade,” ISABE 91-7011, pp. 127-135.

References

- [1] Denton, J.D., 1993, “Loss Mechanisms in Turbomachines,” ASME 93-GT-435.
- [2] Bindon, J.P., 1988, “The Measurement and Formation of Tip Clearance Loss,” ASME 88-GT-203.
- [3] Denton, J.D. and Cumpsty, N.A., 1987, “Loss Mechanisms in Turbomachines,” Inst. Mech. Eng. paper C260/87.
- [4] Booth, T.C., 1985, “Tip Clearance Effects in Axial Turbomachines,” VKI Lecture Series 1985-05.
- [5] Bindon, J.P. and Morphis, G., 1990, “The Development of Axial Turbine Leakage Loss for Two Profiled Tip Geometries Using Linear Cascade Data,” ASME 90-GT-152.
- [6] Heyes, F.J.G., Hodson, H.P. and Dailey, G.M., 1991, “The Effects of Blade Tip Geometry on the Tip Leakage Flow in Axial Turbine Cascades,” ASME 91-GT-135.
- [7] Camci, C., Dey, D. and Kavurmacioglu, L., 2005, “Aerodynamics of Tip Leakage Flows Near Partial Squealer Rims in an Axial Flow Turbine Stage,” Transactions of the ASME Journal of Turbomachinery, Vol. 127, No.1, pp. 14-24.
- [8] Prakash, C., Lee, C.R., Cherry, D.G., Doughty, R. and Wadia, A.R., 2006, “Analysis of Some Improved Blade Tip Concepts,” Transactions of the ASME Journal of Turbomachinery, Vol. 128, No. 1, pp. 639-642.
- [9] Yamamoto, A., Tominga, J., and Matsunuma, T., 1994, “Detailed Measurements of Three-Dimensional Flows and Losses Inside an Axial Flow Turbine Rotor,” ASME 94-GT-348.
- [10] DeCecco, S., Yaras, M.L. and Sjolander, S.A., 1995, “Measurements of the Tip-Leakage Flow in a Turbine Cascade with Large Clearances,” ASME 95-GT-77.
- [11] Patel, K.V., 1980, “Research on a High Work Axial Gas Generator Turbine,” SAE 800618.
- [12] Yaras, M.I. and Sjolander, S.A., 1991, “Measurements of the Effects of Winglets on Tip-Leakage Losses in a Linear Turbine Cascade,” ISABE 91-7011, pp. 127-135.
- [13] Harvey, N.W. and Ramsden, K., 2000, “A Computational Study of a Novel Turbine Rotor Partial Shroud,” ASME 2000-GT-668.
- [14] Dey, D. and Camci, C., 2004, “Tip Desensitization of an Axial Turbine Rotor Using Tip Platform Extensions” VKI Lecture Series 2004-02.
- [15] Kavumacioglu, L., Dey, D., and Camci, C., 2004, “Aerodynamic Character of Partial Squealer Tip Arrangements in an Axial Flow Turbine,” VKI Lecture Series 2004-02.
- [16] Lakshminarayana, B., Camci, C., Halliwell, I., and Zaccaria, M., 1992, “Investigation of Three Dimensional Flow Field in a Turbine Including Rotor/Stator Interaction. Part I: Design Development and Performance of the Research Facility,” AIAA paper 92-3326.